

Article

Ce-Doped-MgAl Superhydrophobic Layered Double Hydroxide for Enhanced Corrosion Resistance Properties

Muhammad Ahsan Iqbal ^{1,*}, Humaira Asghar ² and Michele Fedel ¹

¹ Department of Industrial Engineering, University of Trento, via Sommarive 9, 38123 Povo, Italy; michele.fedel@unitn.it

² Department of Chemistry, University of Torino, via Giuria 7, 10125 Torino, Italy; humaira.asghar@unito.it

* Correspondence: muhammadahsan.iqbal@unitn.it; Tel.: +39-3271749922

Abstract: Double doped layered double hydroxide thin films were developed directly on the aluminum substrate in two steps: Initially cerium-based MgAl-layered double hydroxide (LDH) were synthesized directly on the anodic aluminum surface via the in situ growth method, and were then modified with the stearate anions through an ion-exchange mechanism to achieve compact multi-functional protective thin films. The structural and morphological characteristics of the developed LDH films were investigated, and the surface contact angle measurements (CA) and self-cleaning properties were analyzed. The obtained double doped LDH film displayed the superhydrophobic characteristic with a water contact angle of $\sim 155^\circ$. Furthermore, the superhydrophobic behavior of LDH on exposure to UV radiation ($\lambda = 310$ nm) was examined to evaluate outdoor applications. Long-term Electrochemical Impedance Spectroscopy (EIS) analysis was performed to understand the corrosion resistance properties. The introduction of double doped LDHs demonstrates significantly higher corrosion resistance properties than only cerium-modified LDHs and has shown superior stability against 0.1 M NaCl solution.

Keywords: double doped; superhydrophobic; LDHs; EIS



Citation: Iqbal, M.A.; Asghar, H.; Fedel, M. Ce-Doped-MgAl Superhydrophobic Layered Double Hydroxide for Enhanced Corrosion Resistance Properties. *Solids* **2021**, *2*, 76–86. <https://doi.org/10.3390/solids2010004>

Received: 7 January 2021

Accepted: 11 February 2021

Published: 16 February 2021

Publisher's Note: MDPI stays neutral with regard to jurisdictional claims in published maps and institutional affiliations.



Copyright: © 2021 by the authors. Licensee MDPI, Basel, Switzerland. This article is an open access article distributed under the terms and conditions of the Creative Commons Attribution (CC BY) license (<https://creativecommons.org/licenses/by/4.0/>).

1. Introduction

Aluminum and its alloys are extensively used in a variety of applications due to their good formability, light weight, and high thermal–electrical conductivity properties. However, aggressive solutions are found to disrupt the protective aluminum oxide layer, which causes an initiation of the corrosion reaction and limits their usage in the application ranges [1]. Layered double hydroxides (LDHs) have received considerable attention due to their unique characteristics, like ion-exchange properties, tunable interior architecture, porosity, interlayer distance, and flexible composition range, which make them suitable in numerous fields like catalyst [2], fertilization [3], environmental science [4], adsorption [5], and energy systems [6].

In recent years, layered double hydroxide (LDH)-based coating systems have been thoroughly investigated to substitute the traditional chromate coating systems in order to protect aluminum alloys [7,8]. LDHs are a class of synthetic anionic clays composed of positively charged metal hydroxide layers and interlayer anions. A wide range of divalent metal cations was used to develop M-Al-LDH (M = Li, Ca, Mg, Zn, Ni, etc.) on the aluminum alloys, and the corrosion resistance properties were investigated for LiAl-LDHs [9], MgAl-LDHs [10], ZnAl-LDHs [11], CaAl-LDHs [12], NiAl-LDHs [13], where LDHs have shown the following key features: (a) Active protection due to LDH anion-exchange capabilities; (b) self-healing characteristics; and (c) barrier effect, which inhibits the diffusion of corrosive species to the underlying metal. To further improve the barrier properties, numerous works are reported to develop layered double hydroxide directly on the anodized aluminum surface, where the anodic surface provides the additional protective layer and the source of Al^{3+} for the dense growth of LDH [14]. In recent works, double doped layered

double hydroxide has shown long term corrosion resistance properties, where the synergic effect of corrosion inhibitors demonstrated the self-healing characteristics and multifunctional properties, along with high corrosion resistance properties [15,16]. The current work builds on our previous work [17,18], where we reported the introduction of cerium (III) and perfluorodecyl trichlorosilane species inside the LDH framework to develop double doped LDHs directly on the anodic aluminum source, and a synergetic corrosion protection mechanism was proposed based on the long-term monitoring of EIS and XRD results. However, the stearate-based dopants are further known to improve individual efficiency as corrosion inhibitors in the LDH structure to protect the aluminum surface [19]. The current work is focused on studying the cerium-based LDHs intercalated with stearate groups on the anodic AA6082 alloy, where the stearate endows superhydrophobicity and the cerium act as a corrosion inhibitor, both of which play a significant role in improving the corrosion resistance of LDH. There is no study on such coating modifications, while long-term corrosion resistance investigation will facilitate understanding the combined effect of cerium and stearate addition on LDH stability and performance. The monitoring of long-term corrosion resistance properties and knowledge of superhydrophobicity against the corrosive solution is of valuable significance for a detailed understanding of coatings for practical applications. We focused on the surface superhydrophobicity behavior against UV radiation and different household species for indoor and outdoor coating applications. The relationship between microstructure of superhydrophobic film and anticorrosion performance against corrosive solution is discussed.

2. Experimental

2.1. Material and Methods

Aluminum AA6082 ingot (containing 0.80–1.20 wt.% Mg, 0.15–0.40 wt.% Cu, 0.40–0.80 wt.% Si, 0.25 wt.% Zn, 0.15 wt.% Mn, 0.04–0.35 wt.% Cr, 0.15 wt.% Ti, 0.70 wt.% Fe and balance Al) purchased from Metal Center (Trentino) Italy were cut into the dimension of 1 cm × 1 cm. The samples were mechanically ground with SiC papers of grit 600#, 1200#, 4000# and were washed with deionized water followed by 10 min etching with 0.1 M NaOH solution and further with 0.1 M HNO₃. All the reagents were purchased from Sigma (Aldrich, Milano, Italy).

The cerium-based LDHs were synthesized on anodized aluminum AA6082 according to our previous work [17]. The anodization of the aluminum surface was carried out in 0.1 M H₂SO₄ electrolyte at a constant voltage of 14 V for 30 min at room temperature (25 °C), where the stainless-steel plate was used as a cathode and the pretreated AA6082 specimen acted as an anode (Figure 1). The obtained anodized specimens were vertically immersed in 0.01 M Mg(NO₃)₂·6H₂O (purity ≥ 99.0%), 0.001 CeNO₃·6H₂O (purity ≥ 99.0%), and 0.06 M NH₄NO₃ (purity ≥ 99.0%) mixture solution for 18 h at 80 °C. The pH of the solution was maintained at 10 with a dropwise addition of an NH₄OH (purity ≥ 99.0%) solution and was measured by the pH meter supplied by AMEL Electrochemistry, Milan, Italy. The obtained specimens are named Ce-LDHs.

2.2. Surface Modifications

To obtain the superhydrophobic structure, sodium stearate was used to lower the surface energy. Ce-LDH specimens were immersed in 0.01 M sodium stearate solution at 50 °C for 5 h. On completion, the samples were washed with deionized water and dried in the oven at 40 °C for 4 h. For the sake of simplicity, stearate-modified Ce-LDH is denoted as S-LDH.

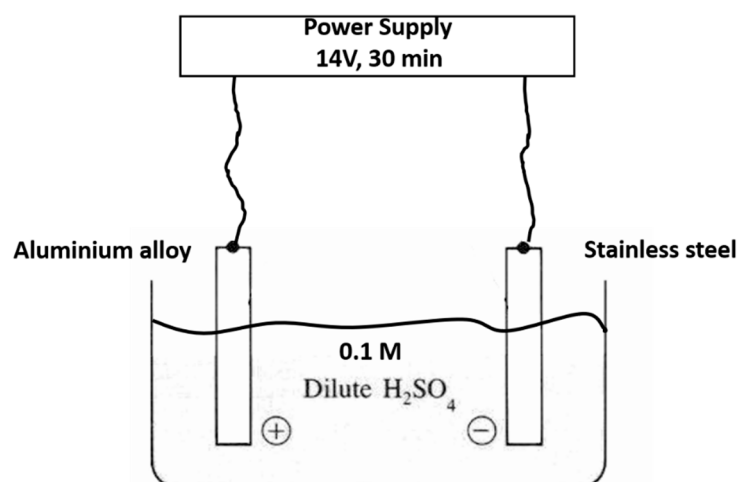


Figure 1. Schematic diagram of AA6082 anodization.

3. Characterization

The surface morphology before and after surface modifications were studied using scanning electron microscopy (JEOL JSM, Tokyo, Japan) at 20 kV accelerating voltage and high vacuum by using the secondary electron mode. The crystalline structure of developed LDHs was investigated using X-ray diffraction (XRD, XRD-6000, Shimadzu, Kyoto, Japan) with Cu K-alpha radiation at 30 kV and 10 mA, $\lambda = 0.1540$ nm. The contact angles (CAs) of LDH measurements were made by acquiring a picture of liquid drops with a digital camera positioned on a static contact angle analyzer. The UV chamber equipped with a 40 w ($\lambda = 310$ nm) high-pressure mercury fluorescent ultraviolet lamp (CO.FO.ME.GRA, Milan, Italy) was used to study the stability of specimens against UV radiation. Digital pictures were also recorded during the self-cleaning process. The corrosion resistance properties were analyzed with Electrochemical Impedance Spectroscopy (AMETEK Meerbusch Germany) by using Parstat-2273 equipment with 0.1 M NaCl aqueous solution at different exposure times with Ag/AgCl/KCl (+210 mV vs. SHE) reference electrode, and platinum as a counter electrode (3.0 mm diameter, 99.95% purity) with an amplitude of 10 mV at the frequency range from 0.01 Hz to 100 kHz.

4. Results and Discussion

The surface morphology of the developed LDH specimens before and after modification with cerium and stearate group is characterized by SEM analysis, as shown in Figure 2a–d. MgAl-LDHs and Ce-LDHs showed curved hexagonal platelet structures grown perpendicular to the substrate and distributed randomly on the surface (Figure 2b,c). The high nucleation density is possibly due to the high concentration of $\text{Al}(\text{OH})_4$ that comes from the anodic aluminum surface, where the sealing treatment of the porous anodic structure by LDH precursors turned the alumina into hydrated alumina. The platelet structure in the case of Ce-LDHs remains unchanged except that the thickness may slightly increase the platelet LDHs. The Ce-LDH precursors also provide a sealing effect for the anodized porous surface. However, after intercalation with stearate groups, the surface morphology changed considerably; the disordered packed platelet structure can be seen in Figure 2d. The intercalation of stearate groups induced considerable stress inside the LDH framework and caused the formation of a disordered packed arrangement. The EDS analysis demonstrated that the mass and atomic percentage ratio of $\text{Mg}/(\text{Al}+\text{Ce})$ is equal to $(31.81/3.56 + 4.44 = 3.97)$ and $(22.7/2.55 + 1.12 = 6.18)$, respectively. The anodic film thickness is around 26.5 ± 1.8 μm , while after the development of Ce-LDHs and S-LDHs on the anodic film, the total film thickness became around 30.6 ± 1.9 and 34.2 ± 1.7 μm , respectively.

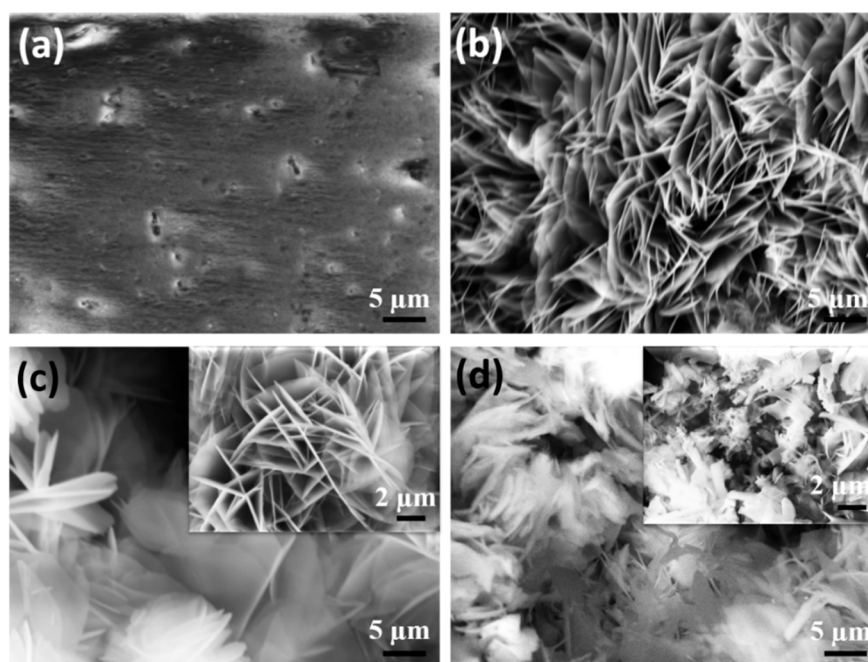


Figure 2. SEM images, (a) anodic AA6082, (b) MgAl-layered double hydroxide (LDH), (c) Ce-LDH, (d) S-LDH.

Figure 3 shows the XRD patterns of MgAl-LDH, Ce-LDH, and S-LDH developed on an anodized aluminum surface. MgAl-LDH reflects the characteristics peak of the LDH structure at 11.8° , 23° , 35° , 61.5° , and 63° , corresponding to (003), (006), (012), (110), and (113) diffraction planes, while on the addition of cerium no distinct difference was observed in reflection peaks. The interlayer thickness (d_{003} , 0.76 nm) and (d_{006} , 0.38 nm) based on Bragg's law were very consistent with the MgAl-CO₃-LDHs [20]. The calculated value of 0.76 nm for d_{003} is characteristic of carbonate intercalated layered double hydroxide and corresponds to $x = 0.33$ with flat-lying anion orientation in the interlayers [21]. The sharp diffraction peak of the (003) crystal plane showed a good preferred orientation and crystal quality concerning LDHs. S-LDH diffraction peaks overlap with that of MgAl-LDHs and Ce-LDHs. No change on the diffraction angle of (003) was observed after modification with stearate groups, except for the decrement in the intensity of corresponding diffraction peaks. This explains the slight weakening of crystal quality after stearate modification and did not make any impact on the crystal structure and interlayer thickness [22]. The intense reflection peaks can further be used to evaluate cell parameters "c" and "a", which can be evaluated by the correlations, $c = (3d_{003} + 6d_{006})/2$ and $a = 2d_{110}$. The cell parameter "c" remains around 2.34 nm; however, in the case of modified MgAl-LDHs, a very slight shift is found for the parameter "a", where 0.302 nm for MgAl-LDHs shifted to 0.300 nm for Ce-LDHs and S-LDHs. The synthesis experiments were performed without a controlled environment and in such circumstances contamination with atmospheric CO₂ cannot be avoided. It is evident that in the case of higher pH value, and without a controlled environment, the potential of formation of carbonate-based LDHs is much higher compared to nitrate-based LDHs. A similar concept has already been explained well in the work of Li, KunWei, et al. [23], where higher pH results in the formation of carbonate-based LDHs, despite the synthesis of LDHs in the nitrate-based solution. It may be assumed that stearate would cause the specific low intensity diffraction peak at $\sim 2.3^\circ$ of 2θ due to diffuse scattering arising [24]; that would be very consistent with the densely packed structure SEM image of the film (Figure 2d).

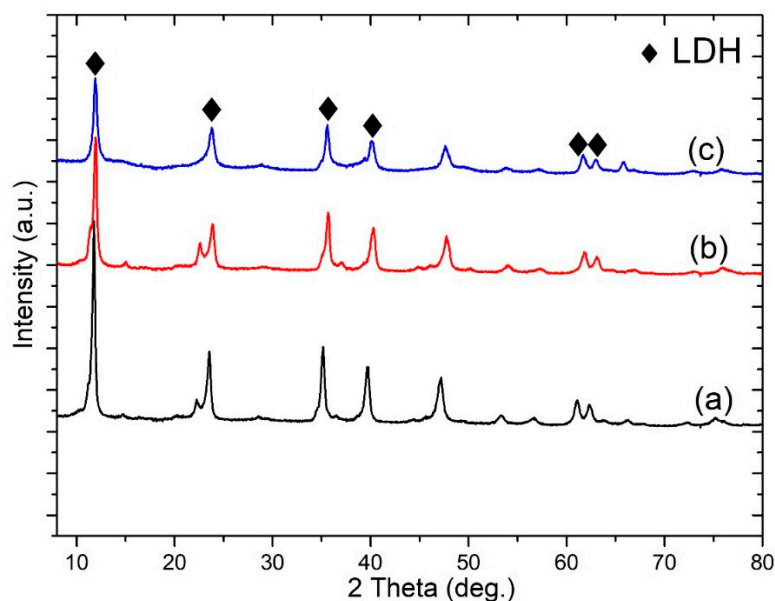


Figure 3. The XRD pictures of LDHs, (a) MgAl-LDHs, (b) CeMgAl-LDHs, (c) S-CeMgAl-LDHs.

The S-LDHs showed superhydrophobic properties with water contact angles (WCAs) of around $\sim 156^\circ$ (Figure 4a). Superhydrophobicity is commonly related to the synergic effect of surface roughness and lower surface energy. Due to the high surface roughness of the LDH structure, the air is trapped within the textured surface and on spikes, resulting in the upper layer of air that modeled Cassie–Baxter regimes, where the liquid–air–solid interaction is superimposed, rather than the liquid–solid model. This causes an increase in superhydrophobic characteristics with substantial-high WCA contact angle hysteresis. It is of great importance to understand the film’s durability against UV radiation and its effect on the superhydrophobicity of the LDHs to evaluate outdoor applications. As can be seen, WCAs exhibited a decline of around 3° after 30 days of exposure with UV irradiation (Figure 4b), indicating strong resistance to UV irradiation, which is well correlated with the literature work [18]. This may be due to the UV-blocking properties of LDH, which resist the UV aging where LDH particle size distribution and layered composition have shown an influential effect on the UV aging properties [25].

As a common indoor coating material, the coating films may be exposed to common household liquids and thus it is important to analyze the domestic liquid-repelling of the LDHs. The digital images of the contact angle measurements against six common household liquid items (tea, acidic drops, basic liquid, corrosive liquids, coffee, and cola) are shown in Figure 5. Liquid droplets in all cases stood on the thin film with a sphere shape and showed good repellency; however, in the case of acidic media, degradation of the thin film was also observed.

Dust contaminations are another parameter to investigate the understanding of self-cleaning properties, where the dust particles cannot be avoided in daily life. To analyze the self-cleaning properties, the graphene-suspended water is used by mixing the graphene in water to evaluate the liquid contamination effect on the film. The graphene suspension was deliberately put on the film surface (Figure 6). It is interesting to observe that the graphene suspension readily rolled away from the S-LDHs without traces on the surface, indicating the well-suited self-cleaning characteristics.

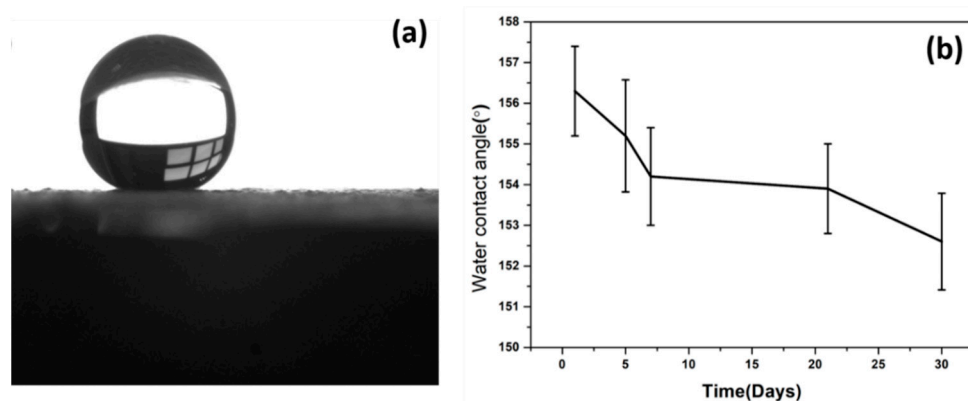


Figure 4. (a) Digital photo of the droplet on stearate-modified Ce-LDH (S-LDH), (b) water contact angles (WCAs) of S-LDH on exposure with UV radiations as a function of exposure time.

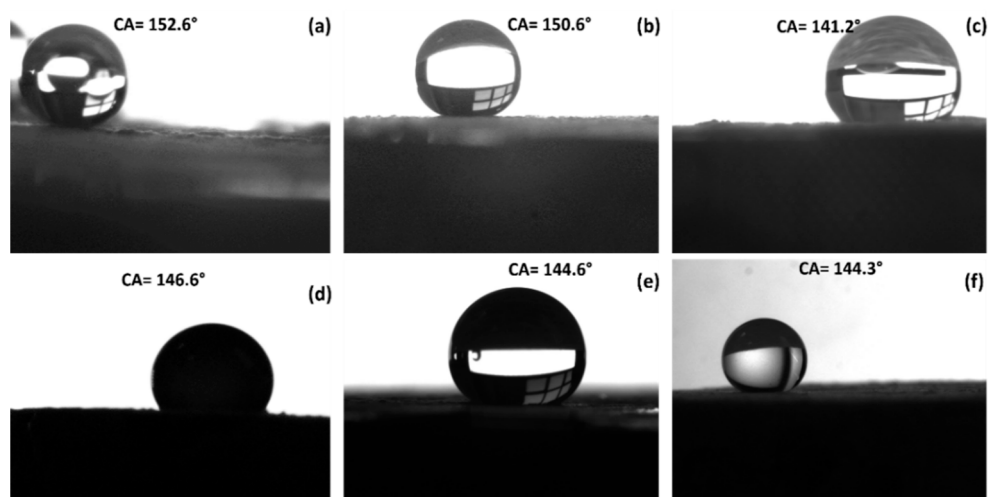


Figure 5. Digital photos and contact angle images of water on different surfaces, (a) 0.1 M NaOH (b) 0.1 M NaCl, (c) acidic solution (pH ~4), (d) coffee, (e) tea, (f) cola.

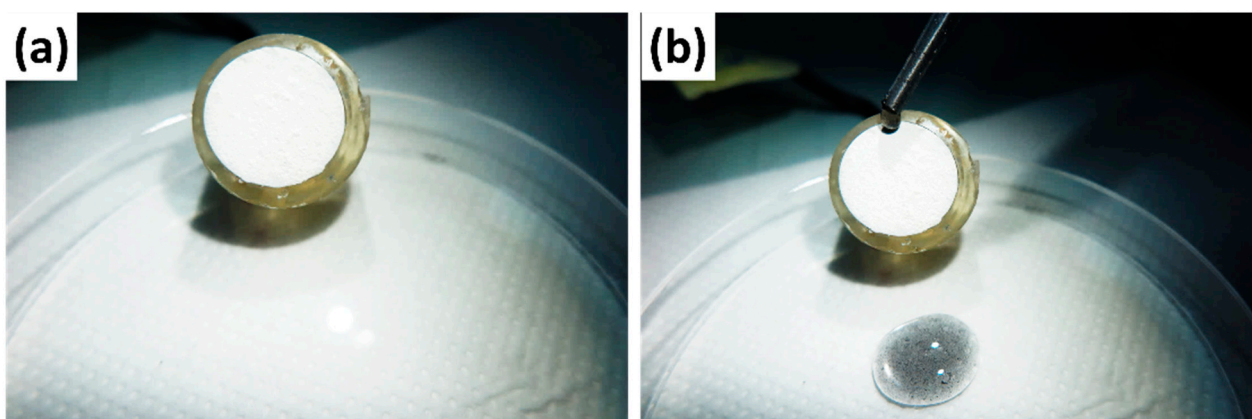


Figure 6. Self-cleaning properties of S-MgAl-LDH; (a) original surface, (b) after graphene suspension.

EIS analysis is a useful approach to understand the influence of superhydrophobic surfaces on the corrosion resistance properties of LDHs. The general protective mechanism of S-LDHs is analyzed through combined results of contact angle measurements and corrosion resistance in long-term immersion in a corrosive solution. Figure 7 shows the

bode plots of developed layered double hydroxide thin films against a 0.1 M NaCl solution. The impedance modulus at the low frequency of 0.01 Hz ($|Z|_{0.01}$) can be used to compare the corrosion resistance of film on contact with the 0.1 M NaCl solution. As can be seen, the impedance modulus is much higher for S-LDH compared to Ce-LDH and MgAl-LDH. It is worth noting that the low-frequency impedance modulus of stearate-modified Ce-LDH is nearly four orders higher than Ce-LDH and six orders higher than virgin MgAl-LDH. In our previous work, Ce-LDH corrosion resistance behavior, a possible protection mechanism, and long term EIS measurements are reported in detail [17]. The improved corrosion resistance properties of cerium-modified LDHs could be due to its precipitation effect on the cathodic sites on contact with corrosive solutions. The higher impedance value of S-LDHs can be ascribed to air film on the superhydrophobic surface, low surface energy properties, the presence of cerium inhibitors inside the LDH galleries, and combined barrier effect of anodic and LDH layers. Furthermore, it is difficult to exchange stearate/carbonate anions with the surrounding chloride anions. The time constant (Figure 7) in the high-medium frequency range corresponds to LDH outer porous network contribution, while in the medium frequency range it exhibits the LDH inner barrier layer contribution in corrosion resistance properties. The stearate-modified Ce-LDH has shown a 40° larger phase angle than Ce-LDH, while it is 70° higher than virgin MgAl-LDH, demonstrating the superior corrosion resistance of S-LDH.

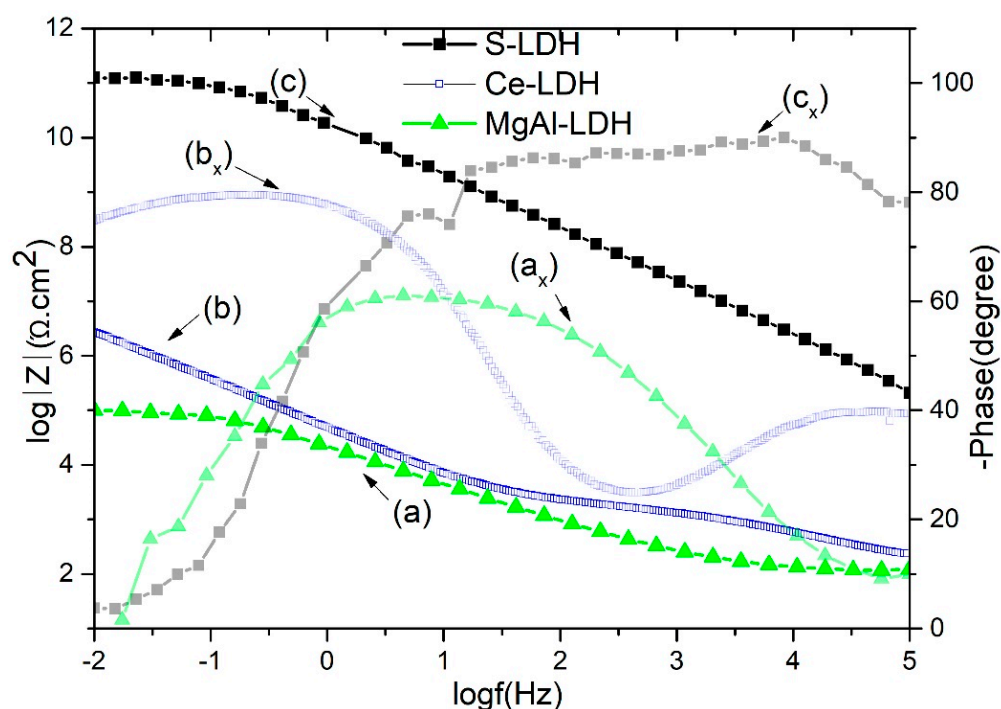


Figure 7. Impedance and phase angle curves of MgAl-LDHs (a and a_x), Ce-LDH (b and b_x), and S-LDH (c and c_x) after 1 h immersion in 0.1 M NaCl solution.

The Bode plots of S-LDHs after various time intervals of immersion (max. 720 h) is shown in Figure 8. S-LDHs demonstrate the impedance modulus of $10^{10.4}$ ($\Omega \text{ cm}^2$) after 24 h of immersion in a 0.1 M NaCl solution, while the impedance modulus has shown a gradual decline in continuous contact with the corrosive solution. The $|Z|_{0.01}$ value of S-LDH reduced from $10^{10.4}$ to about $10^{8.9}$ $\Omega \text{ cm}^2$ after 720 h. The findings describe the higher stability of S-LDH with only a decline of $10^{1.5}$ after a long-time immersion in a chloride's solution. This verifies the low anion-exchange process with chlorides and improved barrier properties that protect the underlying substrate. This long-term stability of the superhydrophobic surface can be ascribed to the presence of stearate, which is stretched outside the surface and is highly efficient in long-term protection. Overall,

different layers of LDH geometry provide a barrier against chloride attack to protect the underlying substrate. The bottom anodic layer is sealed by LDH precursors along with the precipitation of cerium hydroxide/oxides on it, further the final upper air film, and the dense bilayer LDH network sandwiched between them. Stearate-intercalated LDHs repelled the permeation of water molecules and chlorides, which is a key important parameter of that work where stearate introduction causes the lowering of surface energy and endorses superhydrophobic characteristics that enhance the active protection for LDHs; the presence of cerium in the LDH frame protects by its inhibition action through reducing the cathodic reaction rate on contact with corrosive media [26,27]. The strong passive and active protection were found to develop the compactness and integrity of LDHs, which is significant for delaying the corrosion process and is a powerful approach to enhancing anti-corrosion behavior. The Ce (III) addition on LDHs can be subjected to self-healing properties by the formation of $\text{Ce}(\text{OH})_3/\text{CeO}_2$ on protective film degradation. It can be concluded that the stearate plays a role in preventing the attack of aggressive anions; however, the effect was not so conspicuous due to their structural characteristics. As a result, the defect sites were repaired, and corrosion was inhibited efficiently. Two different models are reported to describe the surface wetness in the case of LDH thin films, (a) the Cassie–Baxter model and (b) the Wenzel model, by which the contact angles and wetting natures of the surfaces can be explained. In the Cassie–Baxter model, the air-film on the surface of the film provides the interface for the liquid droplet and the coating film. On the other side, the Wenzel model liquid droplet penetrates the air pockets present in the gap of asperities. Given the susceptibility towards corrosion, air pockets act as an additional layer that hinders the contact of liquid media and solid coating film thus following the Cassie–Baxter model. On the horizontal surface, the chloride solution can remain spherical until the liquid droplet completely dissolves with time. However, on the tilted surface, the droplets will slip off and corrosion resistance properties can further be improved. The superhydrophobic Cassie–Baxter surface on long immersion in a chloride solution may change to Wenzel contact, and thus anticorrosive performance will decline with time, as shown in Figure 9. This is in good accordance with the long-time corrosion measurement (Figure 8).

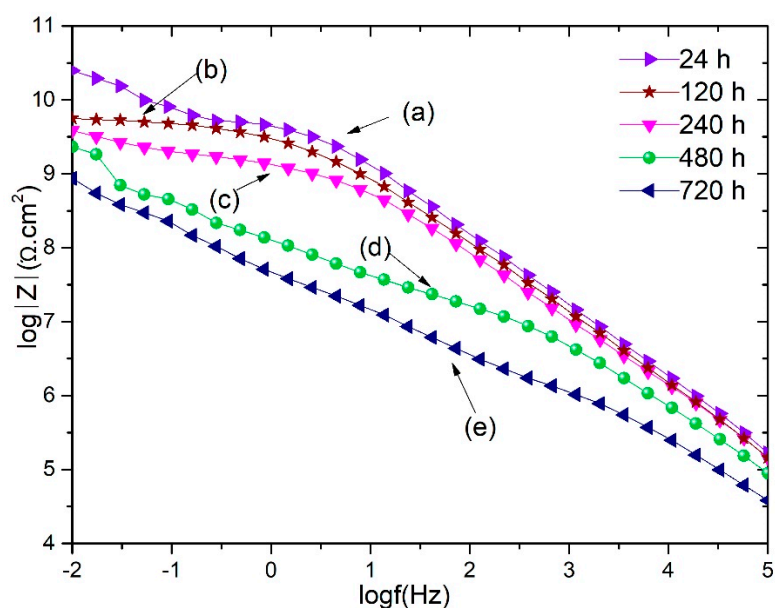


Figure 8. Bode plots of S-LDH at various immersion times, (a) 24 h, (b) 120 h, (c) 240 h, (d) 480 h, (e) 720 h.

Table 1 provides a comparison of the impedance modulus $|Z|_{0.01}$ that can be used to compare the corrosion resistance of film against corrosive solution. The value of $|Z|_{0.01}$ in this work is significantly higher compared to the values in the literature for other

LDH-based coating systems [15,19,28]. However, one must also consider that, (a) a mild electrolyte was used in the current study to monitor the small impedance changes, (b) crystallization time to synthesize LDHs varied in the literature work, that make influence on the film thickness and further on the corrosion resistance properties, (c) the EIS measurements were monitored for different time intervals in the literature studies, and it is difficult to make comparisons with the data.

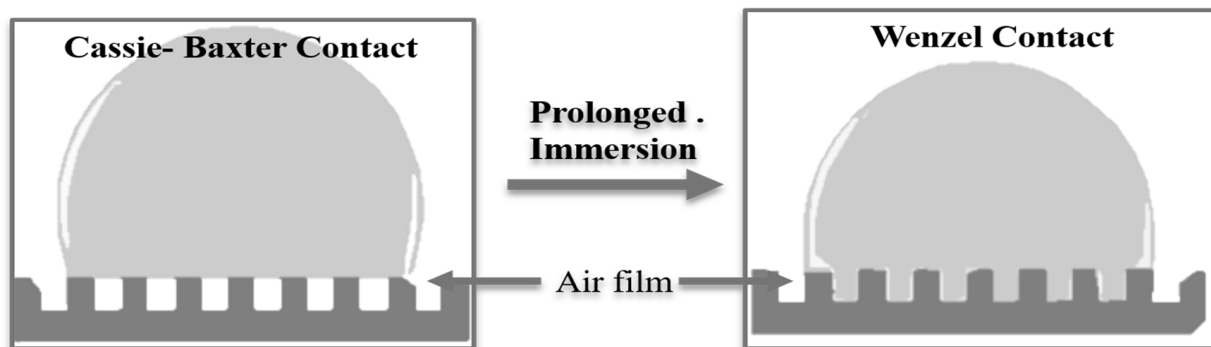


Figure 9. Effect of prolonged immersion time on the surface contact angle.

Table 1. Comparison of the S-LDH with the literature data on aluminum alloys.

LDH	NaCl conc.	Time (h)	$ Z _{0.01}$	REF
ZnAl-LDH-La	3.5 wt%	672	$10^{5.2}$	28
ZnAlCe-LDH-V ₂ O ₇	0.05 M	336	$10^{6.3}$	16
ZnAlVOx-LDH-La	3.5 wt%	1680	$10^{5.8}$	15
MgAlCe-LDH-F	0.1 M	1200	$10^{6.5}$	18
MgAl-S	3.5 wt%	-	$10^{6.3}$	19
S-LDH	0.1 M	720	$10^{8.9}$	This work

La = Laurate, V₂O₇ = Vandate, S = stearate, F = 1H, 1H, 2H, 2H perfluorododecyl trichlorosilane.

The SEM images of S-LDHs and corresponding digital images of water contact angles (WCAs) after different intervals of immersion in the 0.1 M NaCl solution are shown in Figure 10. It is clear that the LDH structure remains intact after 720 h of immersion, and besides of few LDH curvy plate distortions, no other dominant defects were observed. This is well correlated with the EIS long-term immersion results. Stearate intercalated LDHs repelled the permeation of water molecules and chlorides, which is a key important parameter to improve the corrosion resistance properties. The SEM images and gradual decline of impedance modulus are very consistent with the corresponding WCAs. On regular contact with the corrosive solution, there is a decline in the WCAs of the stearate-modified LDHs, but overall the system demonstrates outstanding stability after long term immersion.

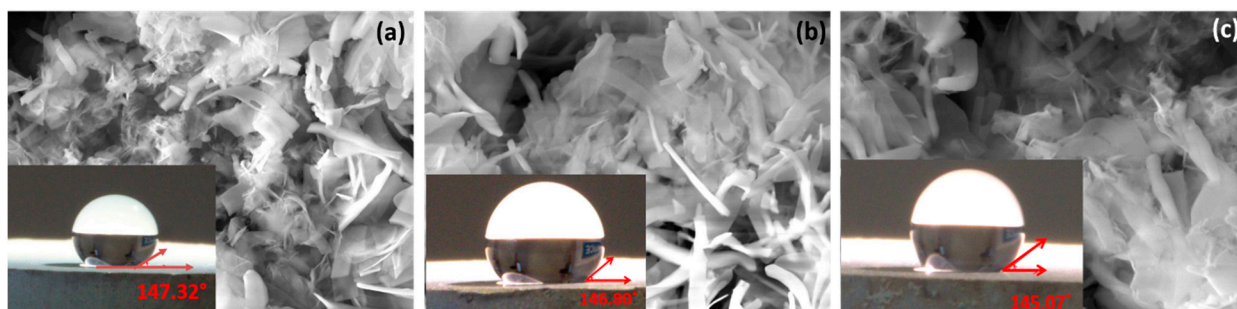


Figure 10. SEM images of S-CeMgAl-LDH after (a) 168 h of immersion, (b) 360 h of immersion, (c) 720 h of immersion in 0.1 M NaCl solution.

5. Conclusions

In this work, stearate-intercalated LDHs modified by cerium were successfully developed directly on the anodic aluminum surface. The introduction of cerium and stearate species in the LDH network was found to enhance the corrosion resistance and long-term stability against the NaCl solution. The developed double doped LDHs have shown superhydrophobic properties with WCAs of $\sim 156^\circ$ and have demonstrated great repellences against common household liquid items. The electrochemical results of S-LDHs indicated strong anti-corrosion characteristics, mainly due to superhydrophobic surface, active and passive protection of stearate-modified Ce-LDHs, and strong barrier of anodic film. The system has shown remarkable long-term stability in the corrosive solution with a $|Z|_{0.01}$ decline of $10^{1.4}$ ($\Omega \text{ cm}^2$) after 720 h immersion in chloride solution, which suggests the developed surface is robust against chemical damages. The obtained S-LDHs also demonstrated great stability against UV radiations. This work sparks the synergic effect of cerium inhibitors and superhydrophobic surfaces to develop a long-term protective structure, applicable for indoor and outdoor applications.

Author Contributions: Conceptualization, M.F., M.A.I., methodology, H.A., M.A.I.; validation, M.F.; formal analysis, M.A.I.; investigation, M.A.I., H.A.; data curation, M.A.I., H.A.; writing—original draft preparation, M.A.I.; writing—review and editing, M.F.; visualization, H.A.; supervision, M.F.; All authors have read and agreed to the published version of the manuscript.

Funding: This research received no external funding.

Data Availability Statement: Not applicable.

Conflicts of Interest: The authors declare no conflict of interest.

References

- Scamans, G.M.; Birbilis, N.; Buchheit, R.G. Corrosion of aluminum and its alloys. In *Shreir's Corrosion*; Elsevier: Amsterdam, The Netherlands, 2010; pp. 1974–2010.
- Xu, M.; Wei, M. Layered double hydroxide-based catalysts: Recent advances in preparation, structure, and applications. *Adv. Funct. Mater.* **2018**, *28*, 1802943. [[CrossRef](#)]
- Benício, L.P.; Eulálio, D.; Guimarães, L.D.; Pinto, F.G.; Costa, L.M.; Tronto, J. Layered double hydroxides as hosting matrices for storage and slow release of phosphate analyzed by stirred-flow method. *Mater. Res.* **2018**, *21*. [[CrossRef](#)]
- Gilea, D.; Lutic, D.; Carja, G. Heterostructures of silver and zinc based layered double hydroxides for pollutant removal under simulated solar light. *Environ. Eng. Manag. J.* **2019**, *18*, 1765–1772.
- Iqbal, M.A.; Asghar, H.; Iqbal, M.A.; Fedel, M. Sorption of As (V) from aqueous solution using in situ growth MgAl-NO₃ layered double hydroxide thin film developed on AA6082. *SN Appl. Sci.* **2019**, *1*, 1–9. [[CrossRef](#)]
- Jing, C.; Dong, B.; Zhang, Y. Chemical modifications of layered double hydroxides in the supercapacitor. *Energy Environ. Mater.* **2020**, *3*, 346–379. [[CrossRef](#)]
- Iqbal, M.A.; Sun, L.; Barrett, A.T.; Fedel, M. Layered double hydroxide protective films developed on aluminum and aluminum alloys: Synthetic methods and anti-corrosion mechanisms. *Coatings* **2020**, *10*, 428. [[CrossRef](#)]
- Bouali, A.C.; Serdechnova, M.; Blawert, C.; Tedim, J.; Ferreira, M.G.S.; Zheludkevich, M.L. Layered double hydroxides (LDHs) as functional materials for the corrosion protection of aluminum alloys: A review. *Appl. Mater. Today* **2020**, *21*, 100857. [[CrossRef](#)]
- Li, J.; Yuan, T.; Zhou, C.; Chen, B.; Shuai, Y.; Wu, D.; Chen, D.; Luo, X.; Cheng, Y.; Liu, Y. Facile Li-Al layered double hydroxide films on Al alloy for enhanced hydrophobicity, anti-biofouling and anti-corrosion performance. *J. Mater. Sci. Technol.* **2021**, *79*, 230–242. [[CrossRef](#)]
- Iqbal, M.A.; Fedel, M. Ordering and disordering of in situ grown MgAl-layered double hydroxide and its effect on the structural and corrosion resistance properties. *Int. J. Miner. Metall. Mater.* **2019**, *26*, 1570–1577. [[CrossRef](#)]
- Iqbal, M.A.; Fedel, M. Effect of operating parameters on the structural growth of ZnAl layered double hydroxide on AA6082 and corresponding corrosion resistance properties. *J. Coat. Technol. Res.* **2019**, *16*, 1423–1433. [[CrossRef](#)]
- Iqbal, M.A.; Sun, L.; LaChance, A.M.; Ding, H.; Fedel, M. In situ growth of a CaAl-NO₃⁻-layered double hydroxide film directly on an aluminum alloy for corrosion resistance. *Dalton Trans.* **2020**, *49*, 3956–3964. [[CrossRef](#)]
- Iqbal, M.A.; Sun, L.; Asghar, H.; Fedel, M. Chlorides Entrapment Capability of Various In-Situ Grown NiAl-LDHs: Structural and Corrosion Resistance Properties. *Coatings* **2020**, *10*, 384. [[CrossRef](#)]
- Kuznetsov, B.; Serdechnova, M.; Tedim, J.; Starykevich, M.; Kallip, S.; Oliveira, M.P.; Hack, T.; Nixon, S.; Ferreira, M.G.; Zheludkevich, M.L. Sealing of tartaric sulfuric (TSA) anodized AA2024 with nanostructured LDH layers. *Rsc Adv.* **2016**, *6*, 13942–13952. [[CrossRef](#)]

15. Cao, Y.; Zheng, D.; Luo, J.; Zhang, F.; Wang, C.; Dong, S.; Ma, Y.; Liang, Z.; Lin, C. Enhanced corrosion protection by Al surface immobilization of in-situ grown layered double hydroxide films co-intercalated with inhibitors and low surface energy species. *Corros. Sci.* **2020**, *164*, 108340. [[CrossRef](#)]
16. Zhang, Y.; Li, Y.; Ren, Y.; Wang, H.; Chen, F. Double-doped LDH films on aluminum alloys for active protection. *Mater. Lett.* **2017**, *192*, 33–35. [[CrossRef](#)]
17. Iqbal, M.A.; Fedel, M. Protective Cerium-Based Layered Double Hydroxides Thin Films Developed on Anodized AA6082. *Adv. Mater. Sci. Eng.* **2020**, *2020*, 1–12.
18. Iqbal, M.A.; Asghar, H.; Fedel, M. Double doped cerium-based superhydrophobic layered double hydroxide protective films grown on anodic aluminium surface. *J. Alloys Compd.* **2020**, *844*, 156112. [[CrossRef](#)]
19. Wang, Y.; Zhang, D.; Lu, Z. Hydrophobic Mg–Al layered double hydroxide film on aluminum: Fabrication and microbiologically influenced corrosion resistance properties. *Colloids Surf. Physicochem. Eng. Asp.* **2015**, *474*, 44–51. [[CrossRef](#)]
20. Evans, D.G.; Slade, R.C. Structural aspects of layered double hydroxides. *Layer. Double Hydroxides* **2006**, *119*, 1–87.
21. Karthikeyan, J.; Fjellvåg, H.; Bundli, S.; Sjøstad, A.O. Efficient Exfoliation of Layered Double Hydroxides; Effect of Cationic Ratio, Hydration State, Anions and Their Orientations. *Materials* **2021**, *14*, 346. [[CrossRef](#)] [[PubMed](#)]
22. Li, Y.; Wu, S.; Dai, Y.; Pang, L.; Liu, Q.; Xie, J.; Kong, D. Investigation of sodium stearate organically modified LDHs effect on the anti aging properties of asphalt binder. *Constr. Build. Mater.* **2018**, *172*, 509–518. [[CrossRef](#)]
23. Li, K.; Kumada, N.; Yonesaki, Y.; Takei, T.; Kinomura, N.; Wang, H.; Wang, C. The pH effects on the formation of Ni/Al nitrate form layered double hydroxides (LDHs) by chemical precipitation and hydrothermal method. *Mater. Chem. Phys.* **2010**, *121*, 223–229. [[CrossRef](#)]
24. Landman, E.P.; Focke, W.W. Stearate intercalated layered double hydroxides: Effect on the physical properties of dextrin-alginate films. *J. Mater. Sci.* **2006**, *41*, 2271–2279. [[CrossRef](#)]
25. Huang, Y.; Feng, Z.; Zhang, H.; Yu, J. Effect of layered double hydroxides (LDHs) on aging properties of bitumen. *J. Test. Eval.* **2012**, *40*, 734–739. [[CrossRef](#)]
26. Mohammadi, I.; Shahrabi, T.; Mahdavian, M.; Izadi, M. Improving the Protection Performance of AA2024-T3 in 3.5 wt% NaCl Solution Using the Synergistic Effect of Cerium Cations and Diethyldithiocarbamate Molecules. *J. Electrochem. Soc.* **2020**, *167*, 131506. [[CrossRef](#)]
27. Wu, W.; Zhang, F.; Li, Y.C.; Zhou, Y.F.; Yao, Q.S.; Song, L.; Zeng, R.C.; Tjong, S.C.; Chen, D.C. Corrosion resistance of a silane/ceria modified Mg-Al-layered double hydroxide on AA5005 aluminum alloy. *Front. Mater. Sci.* **2019**, *13*, 420–430. [[CrossRef](#)]
28. Cao, Y.; Zheng, D.; Li, X.; Lin, J.; Wang, C.; Dong, S.; Lin, C. Enhanced corrosion resistance of superhydrophobic layered double hydroxide films with long-term stability on Al substrate. *ACS Appl. Mater. Interfaces* **2018**, *10*, 15150–15162. [[CrossRef](#)] [[PubMed](#)]